Free Contact Angles in Pitch Bearings and their Impact on Contact and Stress Conditions

Fabian Schwack
Presenting author
Leibniz Universitaet Hannover
Welfengarten 1 A, 30167 Hannover
Schwack@imkt.uni-hannover.de

Matthias Stammler
Co-author
Fraunhofer IWES
Appelstraße 9 A, 30167 Hannover

Heiko Flory
Simulation
IMO Holding GmbH & Co. KG
Imostraße 1, 91350 Gremsdorf

ABSTRACT

The pitch bearing, which connects the hub and the blades, allows the required oscillating movements of the blade, to change the angle of attack thus reducing the lift and drag coefficients there by controlling power and loads of the wind turbine. During the service life of the turbine of approximately 20 years the pitch bearing is loaded dynamically. In a double row four-point contact ball bearing, which is often used for this application, the described loads lead to radial and axial displacements between the inner and outer ring and deformations. These displacements and deformations lead to contact angles which vary from the mounted contact angle which is given by the supplier of the bearing. These divergent angles are called free contact angles. For a four-point contact ball bearing the mounted contact angle in the presented example is 45°. Deviations from the mounted contact angle can lead to reduced fatigue life of the bearing and increased wear, arising from the modified contact behavior. Under axial loads and bending moments the contact area shifts perpendicular to the rolling direction. In the worst case the contact area is truncated, which leads to concentrated and comparatively high stresses.

This paper shows how the free contact angles of a double row four-point contact ball bearing of a modern wind turbine with 7.5 MW behaves during the service life and the effects of contact angle variations to the stress distribution. For the analysis a FE-Model of the bearing which includes the stiffness of the bearing and adjacent components is used.

Keywords

Pitch Bearing, Contact angle, FE-Analyses

1. INTRODUCTION

Modern wind turbines of the multi-megawatt class often use large slewing bearings to connect hub and blades with each other [1]. The most widespread bearing type of these so called pitch bearings are double rowed four-point contact ball bearings. They are able to withstand great axial and radial loads and bending moments [2]. The in comparison to other bearing geometries low costs are also a reason for this bearing choice.

The bearing is used in an oscillatory application. Oscillatory bearing applications are not well researched yet, so that only a few appropriate standards exist [3] [4]. Another problem of the bearing is the, in comparison with the most applications in industry, size of the pitch bearing and low stiffness of bearing and connecting parts. The pitch bearing of the IWT 7.5 reference turbine [5] with a rolling element diameter of roughly 4,5 meters will be used for the analyses. Most standards ([6] and [7]) are not suited for these great sizes or rely on assumptions which lead to deviations between calculated and experimental results. Due to the bearing size, test equipment and execution is expensive, so that tests are limited on small sample sizes. Therefore, detailed FE-Analyses are more important to estimate the expected results on test rigs.

If a ball bearing is highly loaded by axial forces or bending moments or both, the contact angle rises due to displacements, misalignments and deformations [8] [9]. Figure 1 shows the problem in a schematic representation. The bearing in the figure is a four-point contact ball bearing with a mounted contact angle α. On the right side the bearing is axially loaded. This leads to a displacement of the inner ring. The displacement of inner ring in respect to the outer ring leads to an higher value of the contact angle.

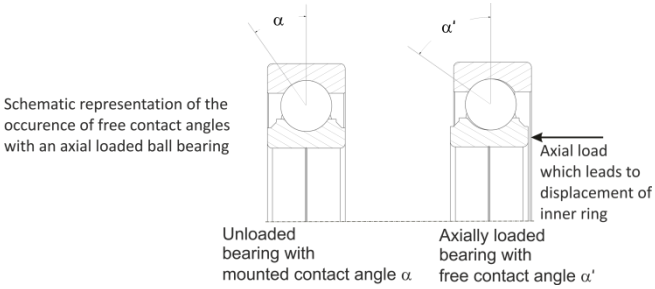

Figure 1: Schematic representation – Free contact angle

The contact angles which are influenced by the loads show deviations in their value to the contact angle which is given by the manufacturer of the bearing. Therefore, the contact angle which is given by the manufacturer is called mounted contact angle. The contact angle which is influenced by the loads is called free contact angle.

The occurring free contact angle leads to contact and stress conditions which differ from the conditions with the mounted contact angle. Furthermore, the bearing properties like the dynamic capacity, the fatigue life and the occurring wear mechanisms are influenced by the free contact angle. For calculations like the calculations of bearing life according to DIN ISO 281 or further calculations according to guidelines and standards like [10] and [11] are only suited for constant contact angles and use therefore the mounted contact angle.

The effect of the free contact angles are part of a variety of publications. Some selected publications are therefore briefly mentioned.

CHEN [12] analysed the load performance of rolling bearings for pitch applications of wind turbines. In this paper a double row four-point contact ball bearing with a diameter of roughly 2,6 m was analysed. The bearing is used in a 1.5 MW wind turbine. Analyses shows the dependency between component stiffness and load distribution and the arising contact angle in pitch bearings. Furthermore, the analyses of the special application shows truncation effects. The stiffnesses were varied to show how design

improvements influence the contact and stress conditions of the pitch bearing.

ZUPAN [13] also analysed large slewing bearings. The focus on this paper was the investigation of a procedure to calculate the free contact angle. The stiffness of the structure was also considered. A further focus of the analyses was the initial play of the bearing. The result of these analyses shows that an initial play of the bearing which is reduced to zero will lead to an equal mounted and free contact angle.

Also different approaches for the FE-Analyses are available in current publications.

DAIDIE [14] determines the free contact angle with a FE-Model. The stiffness in this approach was considered by nonlinear traction springs.

KANIA [15] also presents a FE-Model. In this approach the whole bearing geometry was considered. The model includes nonlinear elastic material properties.

LACROIX [16] presents a model for four-point contact ball bearings with deformable rings. In this paper several methods are proposed which account for the flexibility of the ring in quasi-static numerical models. Furthermore, the bearing and the housing were determined in a semianalytical approach and a FE-model.

OLAVE [17] developed a procedure to determine the load distribution of a four-point contact ball bearing for the structural stiffness. The approach is non linear and needs iterative loops to obtain satisfactory results. OLAVE also build a FE-model to correlate the results of the presented approach.

POTOCNIK [18] analysed the influence from occurring free contact angle and deformations of the bearing ring on the fatigue life of the bearing. With deformations of the ring the fatigue life decreases.

The load distribution in four point contact-ball bearings was analysed in the work of AMASORRAIN [19] . Furthermore, AGUIRREBEITA [20] and POTOCNIK [21] analysed the static load-carrying capacity for the design of a four-point contact ball bearing.

This paper is focused of the analyses of pitch bearing with an outer diameter of 4.69 m which could be used in a 7.5 MW wind turbine. For the analyses the load data were simulated. The contact and stress conditions were analysed with a FE-model, which is not focus of this paper. However, the model will be briefly presented. To consider the stiffnesses of the connection parts, hub and blades, these parts were designed in detail. The results show the free contact angles and their influence on contact and stress conditions for different operating conditions of the turbine.

2. BEARING GEOMETRY AND LOADS

To analyse the occurring free contact angles in a pitch bearing under realistic conditions with a FE-Model, several input data are needed. In detail these are the connection parts, hub and blade, and their stiffnesses and the loads. For this reason the paper uses the data of the reference wind turbine IWT 7.5 MW [5]. The blade geometry is given in the specification of the turbine. With this geometry data the needed stiffnesses of the blades, depending from the load case, are calculated. Furthermore, the hub was designed by the Fraunhofer IWES in close cooperation with the industry.

The bearing geometry is given in Table 1. More information can be found in [3].

Table 1. Bearing geometry [3]

Parameter	Size
Pitch diameter	4690 mm
Ball diameter	80 mm
Contact angle	45°
Number of balls per row	156
Number of rows	2

To receive the stiffnesses of the adjustment structures, in this case blade and hub, realistic CAD-Models were constructed, see Figure 2.

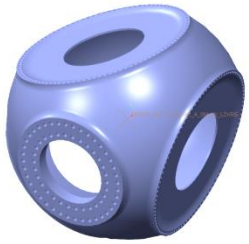

Figure 2: CAD-Model of the hub

The loads need to be separated into normal operating loads and extreme loads. This separation agrees with guidelines and standards [10] [11] which manage the certification of wind turbines. In the following chapters the calculation of the loads are described in detail.

Figure 3 shows a wind turbine under load. The loads are applied in hub-fixed coordinate system according to GL [10]. This means, that the operating direction of the moments and forces are independent from the pitch position of the blades. The used coordinate system is visualised in Figure 4.

Figure 3: Wind turbine under load

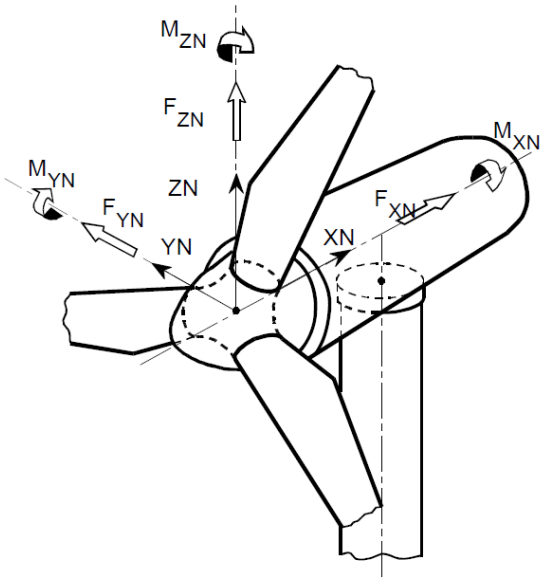

Figure 4: Used fixed-hub coordinate system [10]

2.1 Operating conditions

During normal operation the turbine is connected with the electrical network and converts energy from the wind. The loads where calculated for a turbine life of 20 years and take into account the different wind speeds during this time.

In the foreground of the analyses of free contact angles are the operating conditions while the pitch of the turbine is active. The turbine uses an individual pitch controller which specification can be found in [22] and [23]. Furthermore, the activity of the controller is depicted in [3].

Load conditions are derived with respect to the pitch movements. While the classical analysis of pitch movement is done by LRD (Load Revolution Distributions), a range pair counting is more apt for IPC applications, as amplitude of oscillating movements need to be evaluated. Range pair counting is preferred in comparison to rainflow counting, as every turn in the movement is important for lubricant film conditions [2].

The loads during normal operation can be found in Table 2. This table shows the amplitude range, the number of cycles, the operating time, the mean amplitude, frequency and the equivalent load according to [4]. Every amplitude range will be analysed with the FE-Model to show the free contact angle. The amplitude range portioned in 0,5° degree steps to save computing time while the analyses.

Table 2. Operating conditions [3]

i	Amplitude range [°]	No. of cycles	Oper-ation time [%]	Mean Amplitude [deg]	Mean Frequency [Hz]	Equivalent load [KN]
1	0,05 - 0,55	2,27E+07	14,88	0,22	0,67	9153,89
2	0,55 - 1,05	4,28E+06	4,59	0,75	0,41	8148,75
3	1,05 - 1,55	2,53E+06	3,75	1,30	0,30	7287,11
4	1,55 - 2,05	2,89E+06	5,18	1,80	0,24	7066,84
5	2,05 - 2,55	3,40E+06	7,51	2,30	0,20	6902,72
6	2,55 - 3,05	3,86E+06	8,96	2,80	0,19	6776,68
7	3,05 - 3,55	4,18E+06	10,04	3,30	0,18	6802,57
8	3,55 - 4,05	4,43E+06	10,89	3,80	0,18	6699,16
9	4,05 - 4,55	4,52E+06	11,39	4,30	0,17	6579,67
10	4,55 - 5,05	3,87E+06	9,98	4,79	0,17	6413,73
11	5,05 - 90	4,80E+06	12,82	5,92	0,16	6380,32

2.2 Extreme and special load conditions

The turbine encounters normal operating conditions most of the time. Anyhow, in turbine applications also extreme and special conditions need to be considered. In the given paper it is required that these conditions are also analysed. Table 3 gives an overview of the analysed load cases. The table shows the analysed data set in matrix form. It was analysed at which design load case (DLC) the maximum of one of the moments Mx, My, Mz or one of the forces Fx, Fy, Fz, occurs. The maximum values are marked with a grey background.

Table 3. Used special and extreme conditions

	DLC	Mx [kNm]	My [kNm]	Mz [kNm]	Fx [kN]	Fy [kN]	Fz [kN]
Mx,max [kNm]	**6.1**	35,5	-5,1	-0,1	-0,1	-1,0	-0,5
My,max [kNm]	**1.3**	-1,6	45,6	0,2	1,0	0,3	1,0
Mz,max [kNm]	**5.1**	-6,4	1,9	2,0	0,1	0,3	0,2
Fx,max [kN]	**1.3**	-1,6	45,6	0,2	1,0	0,3	1,0
Fy,max [kN]	**6.1**	-28,1	-3,5	0,4	0,0	1,0	0,3
Fz,max [kN]	**2.3**	1,4	-5,1	-0,1	-0,0	0,0	2,0

For a better understanding of the DLC's a brief overview of DLC 1.3, 2.3, 5.1 and 6.1 is given in Table 4.

Table 4. Overview DLC according to GL [10]

DLC	Conditions
1.3	During DLC 1.3 the turbine is in production. The rotor blades are in an inclined position to the wind. For a three bladed turbine the inclined position is 30° to the wind. This position leads to high edgewise bending moments. This DLC is a special event in production which happened not very often.
2.3	DLC 2.3 assumes an error during production. Therefore, the blades are pitched indiscriminately or the pitch can not act to regulate the load. In this case, the pitch standstill, so that the rpm is very high and the flapwise bending moment arise.
5.1	The turbine was brought to a halt by the emergency shutdown.
6.1	In DLC 6.1 the turbine stands still while the wind blew with 50 m/s. DLC 6.1 is a load case which depicts extreme conditions.

3. FE-MODEL

The respective FE model includes the blade bearing, the hub and one simplified blade root. The parts are connected by bolted joints which are modelled as well. A detailed evaluation of the rolling element loads and contact angles under special load cases necessitates an accurate consideration of the raceway kinematics in the model. Hence, the rolling elements are not simplified at all and consist of hexahedral, deformable elements. These show a surface-to-surface contact to the raceways and show all necessary degrees of freedom to represent the behavior of the real slewing ring. The contact angles and rolling element loads are adjusted, until equilibrium of the system is reached. Even the truncation of the pressure ellipse can be calculated by the simulation due to this detailed modeling strategy. A submodel of the global system is used to evaluate the Hertzian pressure, the sub-surface stress and the deformation of the rolling element contacts. This model is based on a plastic material behavior and contains different material definitions for the hardened layer and the core material.

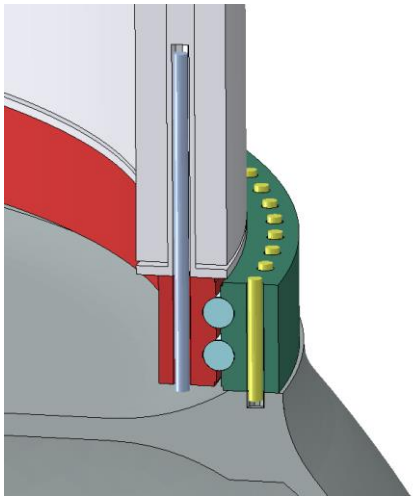

Figure 5: Adjacent Structure in FE-Model

4. ANALYSES RESULTS

In the following sections the results of the analyses will be presented. As mentioned before, the results are presented for the different load conditions. Furthermore, the four raceways of the outer ring are analysed. The labelling of raceways can be seen Figure 6. RW0 and RW1 are the rows of the bearing. AUBottom, AUTop, IRBottom and IRBottom are the four carrying points of the bearing. Due to the equilibrium of forces AUTop and IRBottom are equal. Same applies for AUBottom and IRTop.

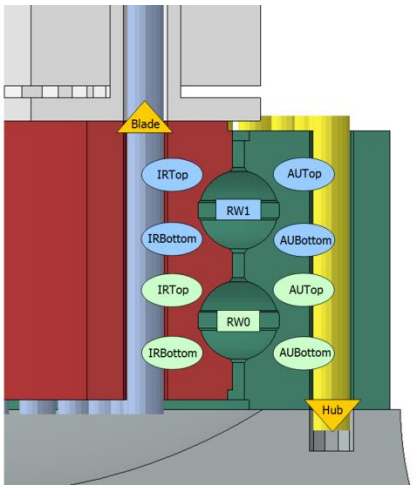

Figure 6: Overview of analysed points

4.1 Results - Operating conditions

The analyses of the normal operating conditions were done according to the 11 operating conditions of Table 2. In the following these operating conditions will be designated OP and listed by their number which can be found in Table 2. Figure 7 shows the individual loads for each of the 156 rollers per row during OP 1. As mentioned before, the analyses were done for the four raceways.

The loads are plotted on their angular position on the raceway. The highest roller loads are roughly 70 kN and can be found at AUBottom RW0, close to the 0° position.

For OP 11 the highest loads can be found near the 350° position. The highest roller loads for this OP are roughly 40 kN, see Figure 8.

The distribution of the rolling element loads depend on the forces and moments which are acting on the bearing. The radial loads of the bearing are in comparison to the axial loads small. Both distributions are not symmetric to 180°. This distribution is mostly influenced by the relationship of the bending moments My and Mx, see Figure 4. For OP 1 My/Mx is roughly 6, so that the My bending moments are dominating. Therefore, the highest rolling element load is close to the 180° position. Higher Mx bending moments would lead to a shifting of the distribution away from the 180° position. This behavior can be seen in Figure 8. For OP 11, My/Mx is roughly 2. Therefore the highest rolling element loads occur close to the 150° position.

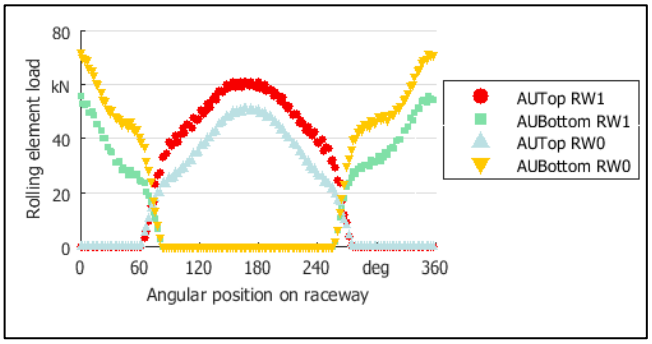

Figure 7 Rolling element loads during OP 1

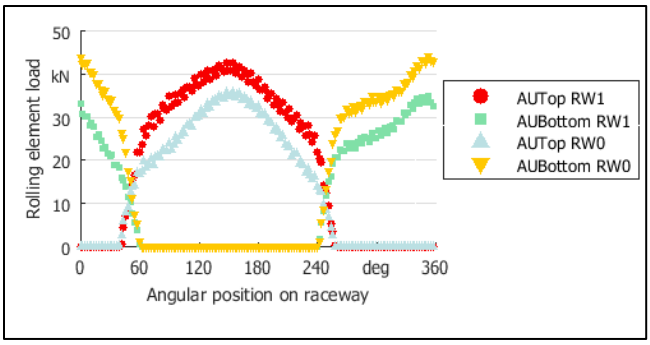

Figure 8 Rolling element loads during OP 11

The contact angles for both OP's are plotted in Figure 9 and 10. For OP 1 the highest contact angle is roughly 65° and for OP 11 roughly 63°, see Figure 9 and 10. The contact angle variation is, as mentioned in the introduction, affected by the elastic deformations of the ring. Therefore, the distributions of the contact angle on the angular position looks similar to the distribution of the rolling element loads. It can be seen, that at roller loads of roughly 30 kN deviations between the free and the mounted contact angle occur.

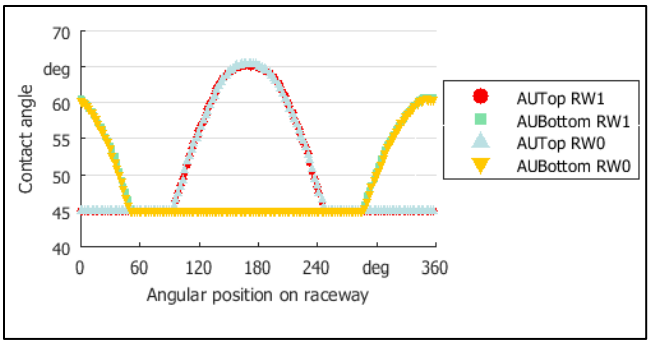

Figure 9 Contact angles during OP 1

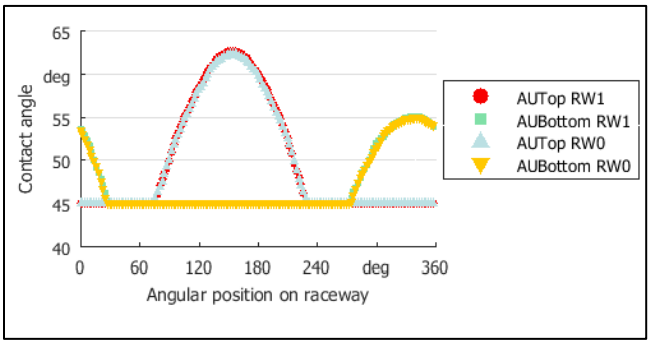

Figure 10 Contact angles during OP 11

Table 5 shows the highest loads which occur for the different OP. Furthermore, the highest free contact angles are given in this table.

Table 5: Analyse results during operating conditions

i	Maximum roller load in N	Maximmum contact angle in deg
1	72168,77	65,67
2	61804,63	64,79
3	53164,60	63,96
4	50608,43	63,71
5	49210,89	63,54
6	48688,93	63,49
7	48313,69	63,42
8	47433,97	63,32
9	46431,99	63,21
10	44732,72	62,98
11	44157,40	62,81

4.2 Results - Extreme and special conditions

The analysis for the extreme and special conditions was done for two special cases. Both cases occur during the simulation of DLC 1.3. It should be mentioned that more than one simulation of this load case was done with different parameter sets. The conditions of these DLC can be found in Table 4. In the first case the resulting bending moment reaches the highest value. In the second case the highest resulting forces occur.

4.2.1 Maximal bending moments

Figure 11 shows the rolling element load and the contact angle in operation of AUTop at RW0 at different peripheral angles on the raceway. As seen before, the forces, and therefore contact angles, are higher for RW1 than for RW0, see Figure 12. Furthermore, the permissible contact angle is given in the figure. The permissible contact angle was calculated using the bearing geometry and the elastic deformation of the bearing during the given load condition. The in comparison high value of My/Mx lead to an distribution which is again nearly symmetric to the 180° position. The highest rolling element load at AUTop RW0 is roughly 110 kN and for RW1 135 kN. For the other points, the rolling element load arises to roughly 170 kN. These high loads leads to free contact angles of roughly 70°. Furthermore, it can be seen, that rolling element loads of roughly 60 kN lead to contact angles which are in value greater than the permissible contact angle.

Same can bee seen in the plot of AUBottom at RW0, see Figure 13. Here the highest rolling element loads of roughly 150 kN occur at the 0° position. This loads lead also to higher contact angles than the calculated permissible contact angle. Same account for the values of RW1 which are plotted in Figure 14.

The contact angle arise to roughly 70°. The highest contact angles lead to truncation. To visualise the effect of truncation, the surface pressure is shown in Figure 15 and 16 in detail. In this figures it can be seen, that the highest surface stresses occur in the truncated area. The pressure, which normally is distributed over the whole elliptical form is now concentrated in a smaller form which is truncated. Figure 17 and 18 shows the effect on the von Misses stresses. The von Misses stresses are also concentrated due to the truncation effect. The detailed view in Figure 18 shows von Mises stresses of 2205 MPa, which is very high compared to the stresses in normal operating conditions.

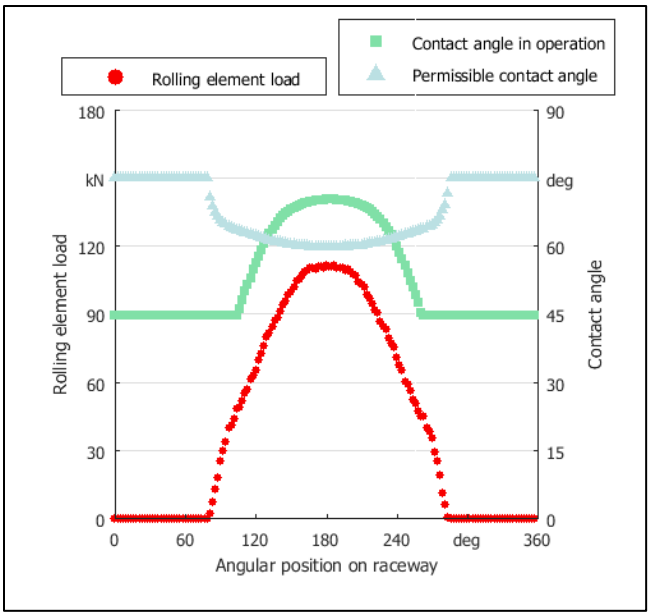

Figure 11 Rolling element load and contact angle of AUTop RW0 during maximal bending moments

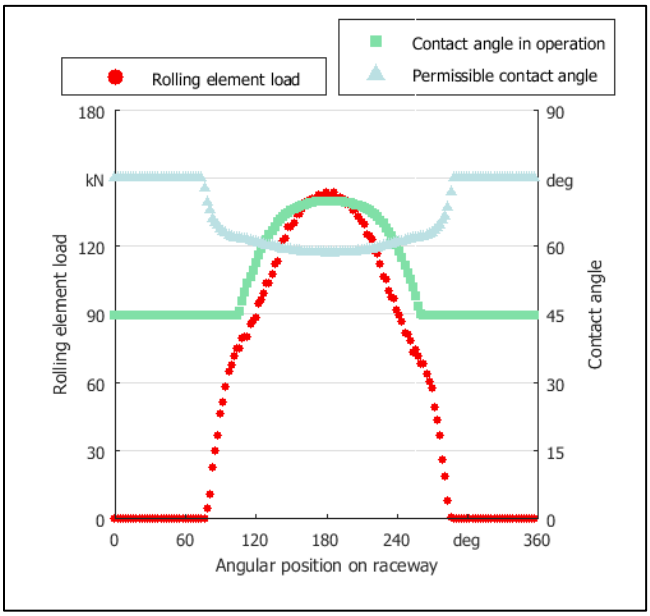

Figure 12 Rolling element load and contact angle of ARTop RW1 during maximal bending moments

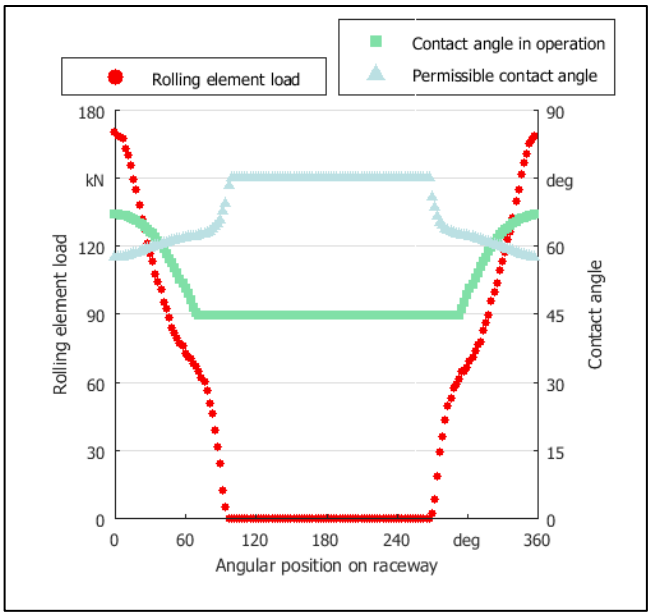

Figure 13 Rolling element load and contact angle of AUBottom RW0 during maximal bending moments

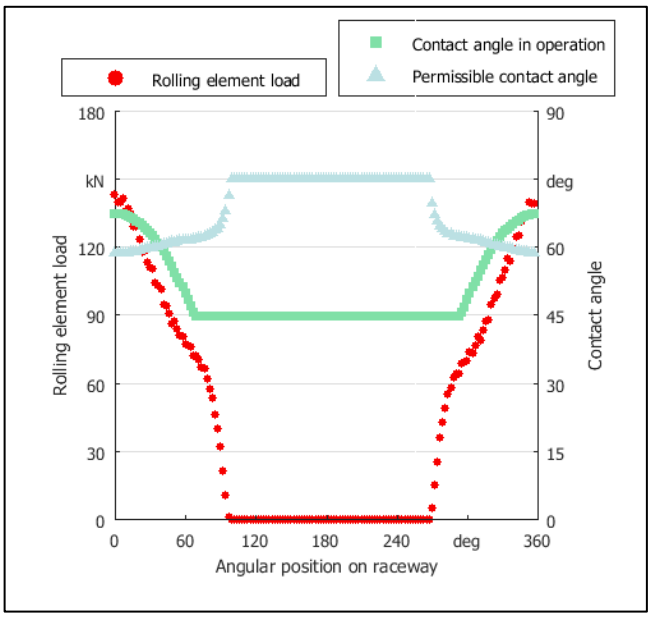

Figure 14 Rolling element load and contact angle of AUBottom RW1 during maximal bending moments

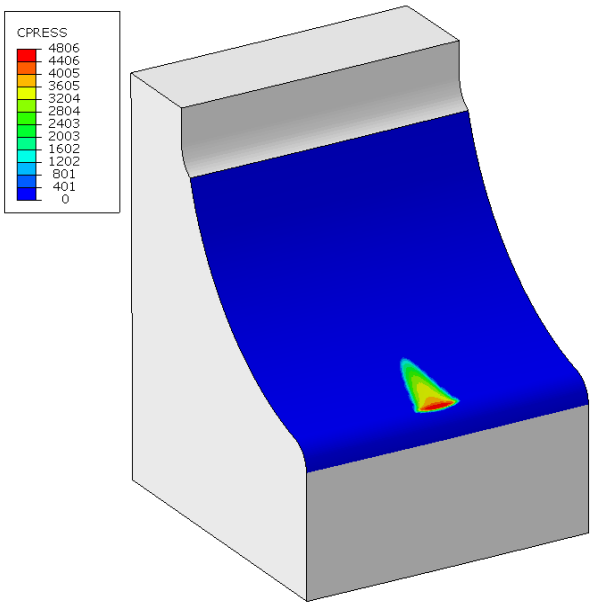

Figure 15: Surface pressure in MPa during maximal bending moments

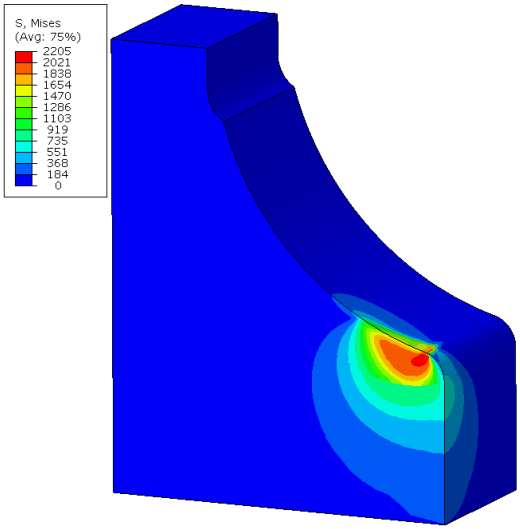

Figure 16: Detailed von Mises stress in MPa during maximal bending moments

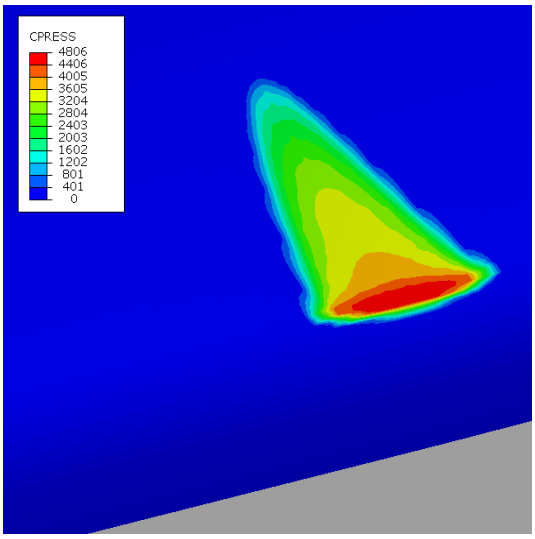

Figure 17: Detailed surface pressure in MPa during maximal bending moments

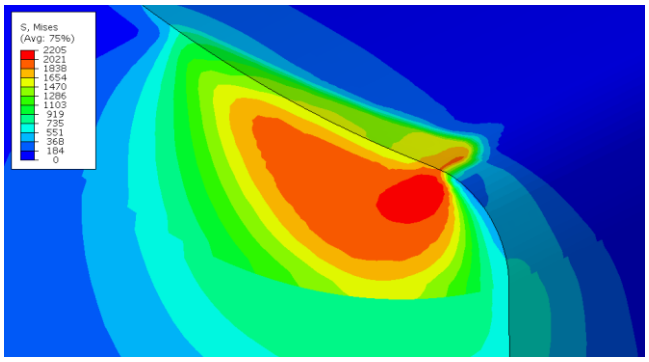

Figure 18: Detailed von Mises stresses in MPa during maximal bending moments

4.2.2 Maximal forces

Due to the occurring maximal bending moment the occurring maximal force were also analysed. The roller loads reach more than 80 kN. In Figure 19 and 20 it can be seen, that the distribution is symmetrical to 270° for AUTop. This can be explained by the load conditions. The Mx bending moments are in comparison very high. Identically to the maximal bending moments the occurring free contact angles, rolling element load and the permissible contact angles are plotted in Figure 21 and 22 for RW0 and RW1 for AUBottom.

Truncation effect can be seen for AUBottom on both raceways. The maximal contact angle is roughly 70°. The truncated contact zone is visualized in Figure 23. The contact pressure is 3937 MPa for this case. Furthermore, the van Mises stresses are shown in Figure 24. The maximum is 1930 MPa.

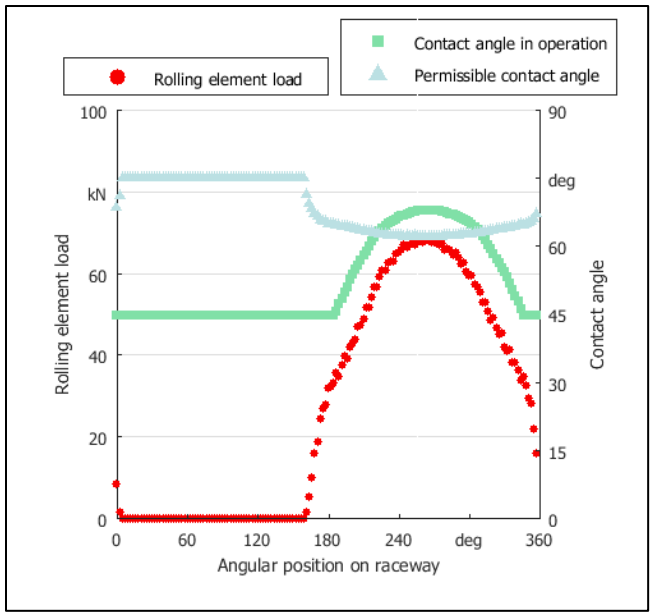

Figure 19 Rolling element load and contact angle of AUTop RW0 during maximal forces

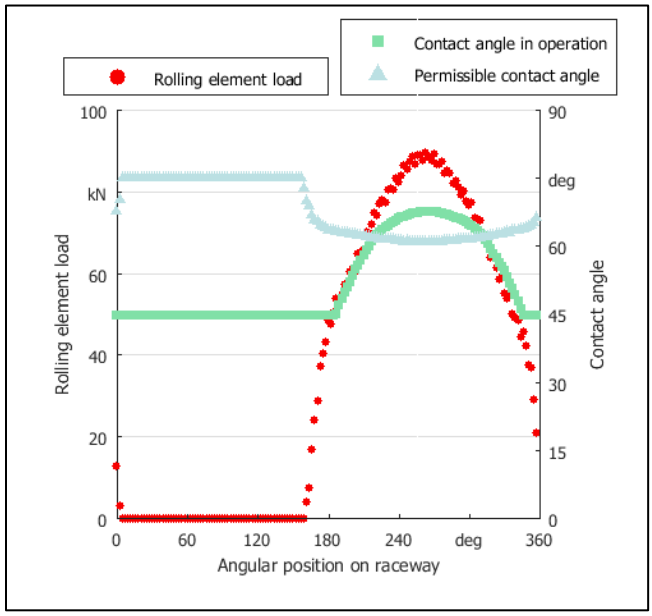

Figure 20 Rolling element load and contact angle of AUTop RW1 during maximal forces

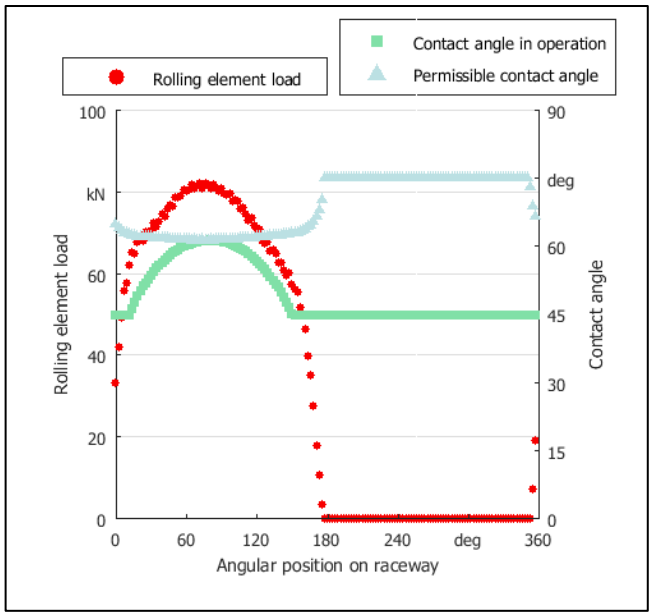

Figure 21 Rolling element load and contact angle of AUBottom RW0 during maximal forces

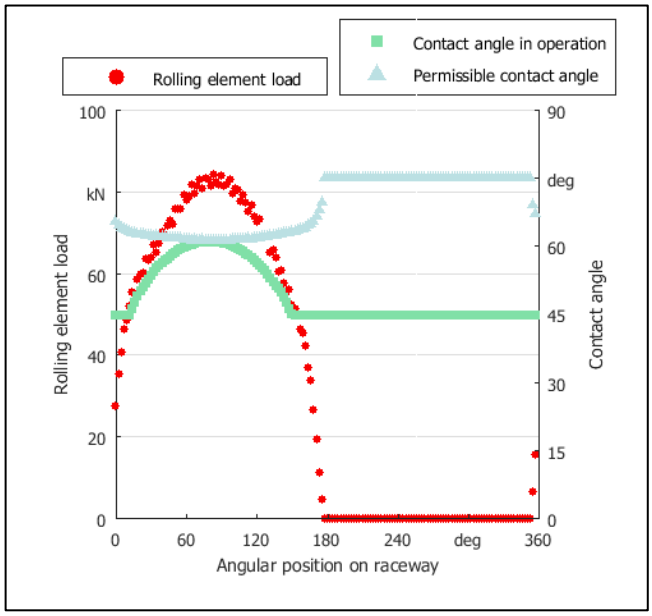

Figure 22 Rolling element load and contact angle of AUBottom RW1 during maximal forces

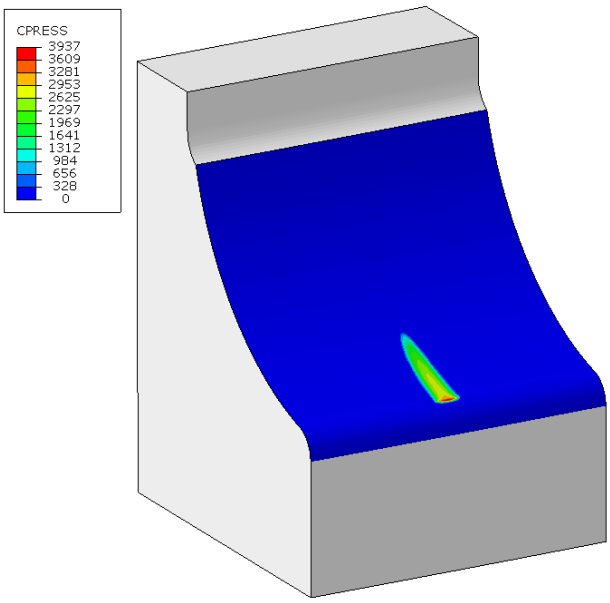

Figure 23: Surface pressure in MPa during maximal Fres

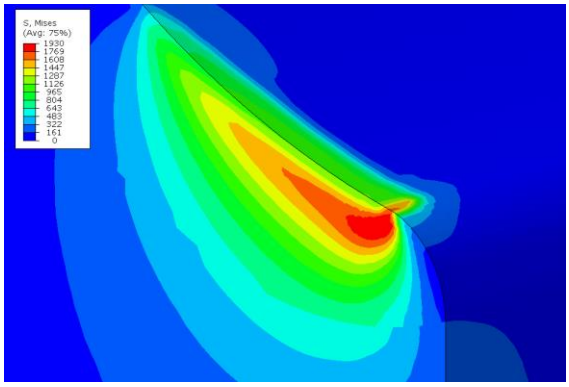

Figure 24: Detailed von Mises stresses in MPa during maximal Fres

5. CONCLUSION

The given paper shows the free contact angles of a pitch bearing of a modern wind turbine with 7.5 MW and the impact of these contact angles on the contact and stress conditions. For the analyses a bearing and connecting parts were designed in detail to consider the stiffnesses. Furthermore, a FE-model were used for the analyses. The loads on the pitch bearing was simulated with HAWC2 and the blades of the reference turbine IWT 7.5. The contact angle was investigated during operating conditions and extreme and special conditions.

Operating conditions

During operating conditions the contact angle rise in average up to roughly 50°. The analyses were done for the four raceways of the outer ring. For OP 1, the OP with the highest equivalent load, the contact angle rises to 65°. During all OP's no truncation effects could be analysed.

Special Conditions

The special conditions were briefly explained. For the critical DLC 1.3 two simulations were chosen which lead to the highest resulting bending moment and the highest forces. The analyses of loads and contact angle were similar done to the analyses of the operating conditions. The highest bending moment leads to free contact angles of roughly 70°. Furthermore, the permissible contact angle was calculated which considers the elastic deformations. In the highest loaded area on angular position of the raceway the free contact angle is given by 60°. Therefore, truncation occurs in this area. To show the effects of truncation in this area, the contact pressure and the von Mises stresses were analysed. The analyses showed that the truncation leads to concentrated and in comparison higher stresses.

During the maximal forces it could be analysed, that truncations effects could occur at both raceways. The maximal free contact angle is given by 65° and the permissible contact angle by roughly 59°. At AUTop RW0 no truncation effects occur.

General

The free contact angle is not considered in most guidelines and standards. The problem to involve the free contact angle in standards and guidelines is the strong dependence on the stiffness of the bearing and the connecting parts. Furthermore, the occurring stresses need to be considered. For most bearing applications the free contact angle is unimportant, because the connection structure, like shafts etc., have good stiffness properties. In the given analyses of a pitch bearing, with in comparison low stiffnesses, the free contact angle needs to be considered.

Furthermore, it could be analysed that for the depicted special conditions truncation effects occur. Truncation leads to concentrated and comprehensively high stresses. These stress spikes need to be prevented for bearing applications. To prevent these effects it could be useful to change the bearing design. This could be done by changing the geometry of the bearing. The loads can be decreased for example by a bigger diameter, a bigger ball diameter or more rolling elements per row.

In most bearing applications it is impossible to change the bearing design. In the given example the bolt circle diameter was given by the geometry of the blade. Therefore it was not possible to increase the diameter. The ball diameter and the number of balls are dependent from each other. Therefore, the best relationship of ball diameter and balls for each row were chosen. Therefore, another option is the use of an completely different bearing design. This could be a four point-contact ball bearing with a different arrangement of the rolling elements or multi row bearings. The effect of the free contact angles occuring in different designs is part of future research.

6. ACKNOWLEDGMENTS

The authors gratefully acknowledge Felix Konstantin Prigge for supporting the research activities presented in this paper and Norbert Bader for the ongoing, technical discussions. Furthermore, the authors would like to thank the German Federal Ministry for Economy Affairs and Energy (BMWi) for funding the project Highly Accelerated Pitch Bearing Test (HAPT) in which this paper arose.

7. REFERENCES

[1] Burton, T., Sharpe, D., Jenkins, N., and Bossamyi, E. 2012. *Wind Energy Handbook*. Wiley & Sons, London.

[2] Stammler, M. and Reuter, A. 2015 - 2015. *Blade bearings: damage mechanisms and test strategies*. Conference for Wind Power Drives, Aachen.

[3] Schwack, F., Stammler, M., Poll, G., and Reuter, A. 2016. Comparison of Life Calculations for Oscillating Bearings Considering Individual Pitch Control in Wind Turbines. *Journal of Physics: Conference Series*, 753.

[4] Harris, T., Rumbarger, J. H., and Butterfield, C. P. 2009. *Wind Turbine Design Guideline DG03: Yaw and Pitch Rolling Bearing Life*. *Technical Report*. NREL/TP-500-42362. NREL.

[5] Sevinc, A., Rosemeier, M., Bätge, M., Braun, R., Meng, F., Shan, M., Horte, D., Balzani, C., and Reuter, A. 2014. IWES Wind Turbine IWT-7.5-164. *Fraunhofer IWES*.

[6] International Organisation for Standardization. 2007. *DIN ISO 281 - Dynamic load ratings and rating life*. Beuth Verlag, Berlin.

[7] American National Standard Institute. 1990. *ANSI/ABMA 9, "Load Ratings and Fatigue Life for Ball Bearings"*. ANSI, 9.

[8] Harris, T. A. and Kotzalas, M. N. 2007. *Rolling bearing analysis*. Taylor & Francis, London.

[9] Houpert, L. 2015. Load-Displacement Relationships for Ball and Spherical Roller Bearings. *J. Tribol.* 2015, 137(2)

[10] Germanischer Lloyd. 2010. *Guideline for the Certification of Wind Turbines*, Hamburg.

[11] IEC. 2005. *Wind turbines - Part 1: Design requirements*. International standard. International Electrotechnical Commission, Geneva, IEC 61400-1.

[12] Chen, G. and Wen, J. 2012. Load Performance of Large-Scale Rolling Bearings With Supporting Structure in Wind Turbines. *Journal of Tribology* 2012, 134.

[13] Zupan, S. and Prebil, I. 2001. Carrying Angle and Carrying Capacity of a Large Single Row Ball Bearing as a Function of Geometry Parameters of the Rolling Contact and the Supporting Structure Stifness. *Mech. Mach. Theory* 2001, 36(10), 1087–1103.

[14] Daidié, A., Chaib, Z., and Ghosn, A. 2008. 3D Simplified Finite Elements Analysis of Load and Contact Angle in a Slewing Ball Bearing. *ASLE Trans.* 2008, 130(8).

[15] Kania, L. 2006. Modelling of Rollers in Calculation of Slewing Bearing With the Use of Finite Elements. *Mech. Mach. Theory* 2006, 41(11), 1359–1376.

[16] Lacroix, S. and Nelias, D. 2013. Four-Point Contact Ball Bearing Model With Deformable Rings. *Journal of Tribology* 2013, 135.

[17] Olave, M., Sagartzazu, X., Damian, J., and Sema, A. 2010. Design of Four Contact-Point Slewing Bearing With a New Load Distribution Produce to Account for Structural Stifness. *Journal of Mechanical Design* 2010, 132(2)

[18] Potočnik, R., Göncz, P., Flaškera, J., and Glodež, S. 2010. Fatigue Life of Double Row Slewing Ball Bearing With Irregular Geometry. *Procedia Engineering* 2010, 2(1), 1877–1886.

[19] Amasorrain, J. L., Sagartzazu, X., and Damian, J. 2003. Load Distribution in a Four Contact Point Slewing Bearing. *Mech. Mach. Theory* 2003, 38(6), 479–496.

[20] Aguirrebeitia, J., Avilés, R., Fernández de Bustos, I., and Abasolo, M. 2010. Calculation of General Static Load-Carrying Capacity for the Design of Four-Contact-Point Slewing Bearings. *J. Mech. Des.* 132, 6.

[21] Potočnik, R., Göncz, P., and Glodež, S. 2013. Static capacity of a large double row slewing ball bearing with predefined irregular geometry. *Mechanism and Machine Theory* 64, 67–79.

[22] Shan, M. 2013. *Field Testing and Practical Aspects of Load Reducing Pitch Control System for a 5 MW Offshore Wind Turbine*, EE-System Conference, Bremen.

[23] Jasniewitz, M. and Geyler, M. 2011. Wind turbine modelling identification for control system applications. *Proc. EWEA*.